Original Article

Journal of Drought and Climate change Research (JDCR)

Winter 2025, Vol. 2, No. 8, pp 31-54

10.22077/jdcr.2024.7510.1067

Removal Efficiency of Sugarcane Bagasse Biochar for Uptake of Sodium Ion from Aqueous Solution: Nonlinear Isotherm and Kinetics Modelling

Jalil Kermannezhad[1], Hassan TorabiPoodeh[2*], Elham Ghanbari-Adivi[3,4], Babak ShahiNejad[5]

1- Ph.D student, Department of Water Engineering, Faculty of Agriculture, Lorestan University, KhoramAbad, Iran.
2- Professor, Department of Water Engineering, Faculty of Agriculture, Lorestan University, KhoramAbad, Iran.
3- Associate Professor, Department of Water Engineering, Faculty of Agriculture, Shahrekord University, Shahrekord, Iran.
4- Nanotechnology Research Center, Shahrekord University, Shahrekord, Iran.
5- Assistant Professor, Department of Water Engineering, Faculty of Agriculture, Lorestan University, KhoramAbad, Iran.
*** corresponding author: ghanbariadivi@sku.ac.ir**

Keywords:
Activation, KOH (Potassium hydroxide), Microwave, Magnetization.

Received:
13 April 2024

Revised:
16 Aug 2024

Accepted:
18 Aug 2024

Abstract

This research examines sodium removability from agricultural wastewater using sugarcane bagasse sorbents, which helps ease the pressure on water resources during droughts. The biochar was produced in an electric furnace, activated with KOH, microwave-heated, and magnetized using a 2:1 ratio of Iron (III) chloride hexahydrate to Iron (II) sulfate heptahydrate. Three KOH-to-biochar ratios, microwave powers, and activation times were used, while sodium concentrations in wastewater samples were adjusted to 2, 4, and 8 g/l with sodium nitrate. Results indicated that higher initial sodium concentrations improved removability. Activated nano biochar achieved 74.4% more sodium removal than non-nano biochar on average. Magnetization reduced sodium removal by an average of 18.8%, with reductions ranging from 10.9% to 31.6%. The activated nano biochar's removability was 1.6 times greater than that of the non-activated version, and magnetization decreased efficiency by 20%. The highest sodium removal occurred at a 3:1 activator-to-biochar ratio during the 200 and 400 W treatments, achieving maximum removability of 61.4% for activated nano biochar and 58.3% for the magnetized version.

How to cite this article:
Kermannezhad, J., TorabiPoodeh, H., Ghanbari-Adivi, E. & ShahiNejad, B. (2024). Removal Efficiency of Sugarcane Bagasse Biochar for Uptake of Sodium Ion from Aqueous Solution: Nonlinear Isotherm and Kinetics Modelling. *Journal of Drought and Climate change Research* (JDCR), 2(8), 31-54. 10.22077/jdcr.2024.7510.1067

Introduction

Irrigation water salinity is a very serious problem in different parts of the world, especially in arid and semi-arid regions. The increasing prevalence of sodium ions in freshwater systems has raised concerns regarding its environmental impact and subsequent implications for water quality. Adsorption has emerged as a promising method for sodium removal from aqueous solutions, particularly with the application of biochar derived from agricultural byproducts such as sugarcane bagasse. This literature review delves into nonlinear kinetic and isotherm models that describe the adsorption processes of sodium ions onto modified sugarcane bagasse biochar. The use of saline water in agriculture can have significant environmental, economic, and social consequences. Irrigating with saline water increases the concentration of salts in the soil, which can lead to soil salinity. This reduces the ability of plants to absorb water and nutrients. Excess salts in the soil can hinder plant growth and performance. Plants experience stress in saline conditions, which may cause them to weaken or dry out. Salinity can decrease the yield of both agricultural and horticultural products. Additionally, the quality of produced goods is also affected. Also it can affect the physical and chemical properties of the soil, leading to changes in water behavior, such as permeability and water-holding capacity (Ehtaiwesh, 2022). Additionally, the rising demand for fresh water driven by population growth will intensify pressure on water resources in the future. This will make the reliance on saline and unconventional water sources a significant concern, particularly in regions already experiencing water scarcity. Meanwhile, agriculture, the largest consumer of water globally, suffers from the use of saline water, which not only diminishes crop yields but also degrades soil structure and harms the environment. Although such measures as leaching, local irrigation, cultivating saline-water-resistant crops and saline-fresh-water mixing can enable the use of saline water in irrigation, they have short-term effects and cannot fully solve the salinity problem (Ayers & Westcot, 1985; Siyal et al., 2002; Dudley et al., 2008; Naik & Panda, 2008). The wastewater desalination and its reuse is a relatively new approach in the water industry that solves saline-water problems through various methods, but it is uneconomical due to high equipment costs and energy consumption especially in agriculture where water consumption and costs are much higher. Adsorption is a process in which one substance becomes incorporated into another, typically involving a liquid adsorbing a gas or a solid absorbing a liquid or gas. It is distinct from adsorption, where molecules adhere to a surface. In environmental science and engineering, absorption is often

utilized to remove contaminants from air or water through various materials known as adsorbents (Pourhakkak et al., 2021). Common adsorbents used in these processes include activated carbon, zeolites, and resins. Each of these materials has its own strengths and weaknesses when it comes to capacity, selectivity, and environmental impact (Crini et al,. 2019). Activated carbon, zeolites, and resins are traditional adsorbents used for various applications such as water purification. Activated carbon is effective for adsorbing organic compounds but is costly to produce and maintain. Zeolites are useful for ion exchange, yet they may not remove organic contaminants, and high-quality varieties can be expensive and scarce. Resins are synthetic polymers that remove ions but are sensitive to pH and temperature, which can hinder their effectiveness, and their production poses environmental concerns. Overall, while these materials are valuable, they have significant limitations that may affect their practical applications (Yılmazoğlu, 2021).

Kinetic studies are essential for understanding the adsorption rates and mechanisms. Commonly used models include pseudo-first-order and pseudo-second-order kinetics. According to Ho and McKay (2000), pseudo-second-order kinetics often provides a better fit for adsorption data, indicating that chemisorption may be the rate-controlling step. Nonlinear regression techniques allow for more accurate parameter estimation in the context of adsorption kinetics. Nonlinear forms of the pseudo-second-order model have been utilized, leading to improved fit and understanding of the dynamics involved in adsorption (Revellame et al., 2020; López-Luna et al., 2019).

The understanding of how sodium ions interact with biochar under equilibrium conditions is crucial. Langmuir and Freundlich models are often employed. The Langmuir model assumes monolayer adsorption on a surface with a finite number of identical sites, while the Freundlich model is an empirical equation indicating multilayer adsorption. Recent work by Kasraee et al. (2022) highlights the applicability of nonlinear forms of these models in assessing adsorption behavior.

Nonlinear isotherm modeling allows for the fitting of adsorption data without linearization, which can introduce bias. By employing nonlinear regression analysis, researchers have observed better predictive capabilities in characterizing sodium uptake in MPPMC (the modified Pinus massoniana pollen microcarriers) systems (Li et al., 2024).

Factors such as pH, temperature, and modification techniques significantly impact the efficiency of sodium ion adsorption. Modifying sugarcane bagasse

through chemical alteration enhances the surface area and functional groups available for ion exchange (Mubarak et al., 2024).

The use of modified sugarcane bagasse biochar proves to be a viable option for sodium removal, supported by rigorous nonlinear kinetic and isotherm modeling. The effectiveness of adsorption depends on various factors, and continuous research into these mechanisms clarifies the pathways that lead to improved environmental remediation techniques.

As activated carbon is made from such inexpensive materials as wood, coal, oil, coke, sawdust and plant waste, it is quite economical and highly capable of removing a wide range of organic and inorganic pollutants from aquatic and gaseous environments (Wu et al., 2008; Jamil et al., 2010; Mehrabinia and Ghanbari-Adivi, 2022; Mehrabinia et al., 2021).

Natural materials and agricultural/ industrial wastes are effective and low-cost adsorbents due to their functional groups like hydroxyl and carboxyl. However, accurately predicting their adsorption processes is challenging because of their complex chemistry, requiring a deep understanding of the interactions involved (Kietlinska & Renman, 2005; Oliveira et al., 2005). Agricultural by-products primarily consist of cellulose, which, when submerged in water, acquires a negative charge and interacts with cations, leading to significant adsorption capacity for various cations (Shang et al., 2003). Rahal et al. (2023) investigated the removal of sodium ions from water by using date pits activated with sulfuric acid. They investigated the effect of activation time, initial sodium concentration, contact time and pH on sodium removal. The specific surface areas of natural and activated date pits were measured as 645.46 and 825.03 m^2/g, respectively. According to their results, the maximum sodium absorption capacity was observed at a contact time of 90 min, the initial concentration was 600 mg/l, the pH was 9.0 and the adsorbent dose was 0.1 g/l. Their findings showed that the Freundlich isotherm model and the pseudo-second order model had the best agreement with the measured values. Hettiarachchi et al. (2016) studied the efficiency of the phosphoric acid-activated coconut straw biochar in removing sodium and magnesium ions from saline water and showed that the removal rate of these ions from NaCl and $MgCl_2$ (0.2 mol/dm^3 standard solutions) was about 50%, which increased to 80 and 72%, respectively, under repeated filtrations. Musie et al. (2023) investigated the removal of sodium ions from water by using raw bean husk and raw bean husk activated with sulfuric acid. They investigated the ability to remove sodium ions by treated raw bean husk with different activation time and

concentrations of sulfuric acid. The initial concentration of sodium ions in their study was 1643 mg/l and the absorbent ratio of the adsorbent was 12.5 g/l. According to their results, the maximum removal was 27.8% for the activator concentration of 4 mol/l and the contact time of 6 hours. Also, the BET results for bean husk and activated bean husk were measured as 0.67 and 0.44 m^2/g, respectively. According to their results, the optimal removal results for bean husk and activated bean husk for a contact time of 3 hours, a pH equal to 10, an initial concentration of sodium of 3486 mg/l and an adsorbent dosage of 0.5 g/L were measured as 20.7% and 17.23%, respectively. They also reported that the Langmuir model and the pseudo-second-order model had the best agreement with the measured values.

Kharel et al. (2016) investigated the effectiveness of wheat and rice husk ashes in reducing water hardness, with hardness levels ranging from 236 to 580 mg/l and ash concentrations from 2.5 to 25 g/l. They found that wheat husk ash achieved the highest reduction of 81% (67 mg/g) at 17.5 g/l, while rice husk ash reduced hardness by 58% (44 mg/g) at 22.5 g/l. Increasing the ash concentration beyond these levels did not further reduce hardness. Wheat husk ash was more effective due to its higher content of alkali metal oxides. Although both ashes reduced water hardness, they did not render the water drinkable because of increased alkalinity. Singh et al. (2017) studied the sodium adsorption ratio (SAR) reduction rate in saline water and showed that it was 27.83, 25.52, 22.21 and 15.46% for paddy husk ash, paddy straw biochar, activated biochar and coco peat, respectively; the equilibrium contact time for all absorbents was 15 min. Doing columnar tests on combined rice paddy husk-laterite soil filters, Chowdhury et al. (2022) used columnar tests on combined rice paddy husk-laterite soil filters to see how they affected lowering the salinity of the water. They found that the average rate was 26.61 and the highest rate was 42.86%. Bindhu et al. (2021) studied the water-hardness-reducing effects and found that the highest rates, after 3 hours of contact time, were 84.38, 62.5 and 31.25% for 2, 20 and 1 gr of potato powder, coconut activated carbon and wheat husk ash, respectively.

Studies conducted so far on removing sodium from effluents by such low-cost adsorbents as agricultural/industrial wastes are limited. This study investigates the sodium removability of agricultural wastewater using sugarcane bagasse adsorbents. Also, it investigates the effectiveness of activated nano biochar, non-nano activated biochar and magnetic nano biochar in sodium removal. Assess the impact of different activation methods and conditions, including ratios of KOH to biochar, microwave powers, and activation

times, on the sodium removal efficiency investigated. The main objective of this study is to investigate the linear and nonlinear isotherms and kinetic behavior of sodium ion adsorption using chemically treated magnetic activated carbon synthesized from sugarcane bagasse waste. Further research suggested approaches include experimenting with different treatment methods, such as acids or heating, and combining bagasse with other natural adsorbents. Additionally, the impact of environmental factors like temperature, pH, and contact time on salt removal efficiency should be investigated. Finally, testing various forms of sugarcane bagasse, such as powder or pellets, can help identify the most effective form for adsorption.

Materials and methods

1.Materials

Sugarcane bagasse (SB) was provided by Hakim Farabi Agro-Industry Co., a sugar mill in Khouzestan Province (48_360E, 30_590N), southwest of Iran. NaOH (99.0 wt%), potassium hydroxide (KOH, 85.0 wt%) and hydrochloric acid (HCl, 38 wt%) were purchased from MERCK Co. Nitrogen (99.999%) was supplied by Wuhan Zagrosgas Air & Gas Co.

To prepare the biochar, this research used the sugarcane bagasse as a primary biomass by: 1) washing it several times with ordinary and distilled water and drying it in the open air to remove its remaining salts; 2) crushing it with an industrial mill and placing it in an oven at 60 °C for 24 hours to remove its excess moisture; 3) grinding the crushed bagasse with a small mill for further milling; 4) passing it through 60 and 100 mesh sieves in two stages for more uniformity and 5) placing it in closed containers (Nie et al., 2018).

1.1.Biochar

Biomass was converted to biochar (BC) using a heat-programmable electric furnace, where the temperature rise was set at 5 ° C/min for a uniform heat distribution. Bagasse was placed inside a steel reactor, into which nitrogen gas was injected at a fixed flow rate and prevented it from oxidation. Biomass was kept at 600 ° C for 2 hours thereafter, the furnace was turned off while nitrogen gas was injected, and the temperature was slowly lowered to that of the lab (Iwuozor et al., 2022). Considering the sizes of the furnace and reactor, each time 20 gr of biomass was placed in the reactor and about 5 gr of biochar was produced after the carbonization process, the biochar production efficiency under these conditions was about 25%.

1.2.Nano biochar

Nano biochar (N-BC) was produced by a planetary ball mill with ceramic cup and bullets (Figure 1), where the bullet-to-biochar weight ratio was 15:1 and the rotation speed was 300 rpm (Kathiresan

& Sivaraj, 2016; Mehrabinia et al., 2022). The useful mill-activity time was 2, 4 and 6 hours and it worked for 3 minutes and rested for 1 minute to prevent the temperature to rising and cohesive masses to forming in the samples; As size and uniformity of particles were important, use of a gradation device was made.

1.3.Activated nano biochar

1.3.1.Chemical reaction with activator

Chemically activated nano biochar was produced using KOH with weight ratios of 2:1, 3:1, and 4:1. For different ratios, KOH was dissolved in deionized water in separate containers and then biochar was added to the solution. The suspension was stirred on a hotplate for 2 hours at 80 ° C, kept at room temperature for 24 hours and then dried in the oven for another 24 hours at 105 ° C.

1.3.2.Activation in microwave

To activate the KOH-nano biochar mix, a domestic microwave oven with adjustable time and power settings was used (Nasri et al., 2017). The microwave chamber was isolated, with only two openings for nitrogen gas to enter and exit, creating an inert atmosphere. The samples were microwaved under nitrogen for varying durations (5, 10, and 15 minutes) and power levels (200, 400, and 700 watts). Afterward, they were washed multiple times with hot deionized water to achieve a neutral pH post-pyrolysis. Finally, the activated nano biochar (AN-BC) samples were dried at 105° C for 24 hours.

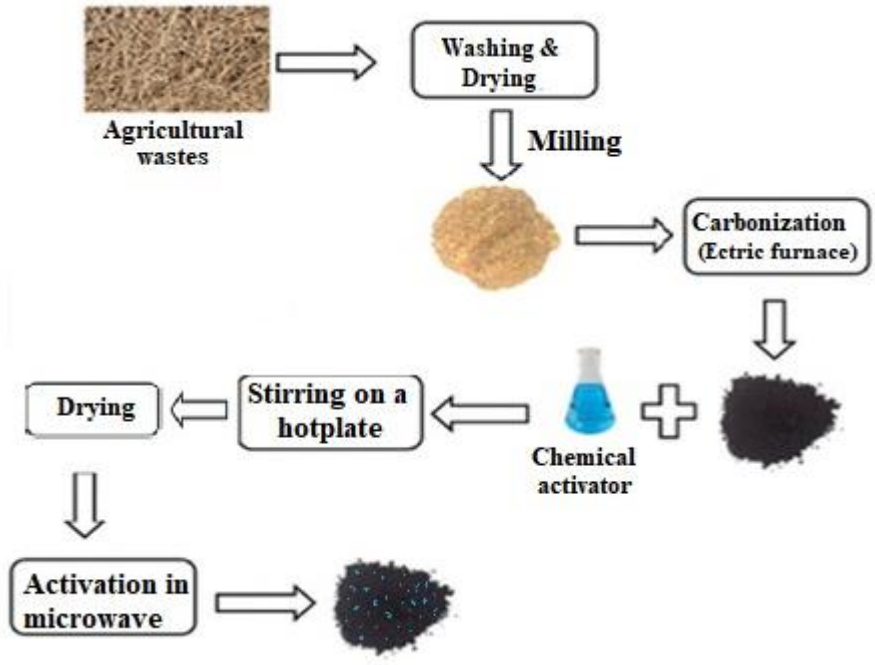

Fig 1. Schematic of production stages of active biochar

1.4.Magnetic biochar

To magnetize adsorbents using Nasri et al. (2017) and Wu et al. (2018) methods, magnetic activated nano biochar (MKN-BC) was produced using iron (III) chloride hexahydrate and a 0.05 mol/l magnetic suspension of iron (II) sulfate heptahydrate (1:2 ratio). The KN-BC was mixed with the magnetic suspension and stirred at 6 rpm for 2 hours at 80 ° C, and the samples were dried for 24 hours at 105 ° C.

1.4.1.Activation in microwave

The initial biochar was subjected to microwave treatment at power levels of 200, 400, and 700 watts for durations of 5, 10, and 15 minutes, with nitrogen gas introduced during the activation process. To enhance the specific surface area of the biochar, following the methods of Wu et al. (2015) and Cheng et al. (2017), deionized hot water was immediately added to the sample container post-activation. The adsorbents were then repeatedly washed with this water to achieve a neutral pH. The MKN-BC samples were subsequently dried in an oven at 105°C for 24 hours.

In this study, the abbreviations BC, Ka-BC, KaN-BC, and MKaN-BC refer to biochar, activated non-nano biochar, activated nano biochar, and magnetic activated nano biochar, respectively. The index ‘a’ indicates the KOH/BC ratio. The microwave power and activation duration are denoted by two numbers following the adsorbent name; for example, MK3N-BC-400-10 signifies magnetic activated nano biochar with a KOH/BC ratio of 3, microwave power of 400 watts, and an activation period of 10 minutes.

1.5.Drainage samples

Saline samples were taken from sugarcane drains where the sodium content was about 4 g/l and the amount of sodium in the samples was set to be 2, 4 and 8 g/l using sodium nitrate and deionized water.

Bach tests

To assess the sodium removal capability of the produced adsorbents from drainage, the batch (discrete) method was employed. In this method, 0.75 g of the adsorbent was added to 50 ml of water. The mixture was stirred on a shaker at 150 rpm for 12 hours, then filtered through paper to measure the sodium content. A total of 729 samples (with three iterations) were used to evaluate the sodium removal efficiency of the adsorbents. Additionally, 138 samples were utilized to study the kinetics and isotherms related to the removal process using MK_3N-BC-400-10.

Physical and chemical parameters

A flame photometer was used to measure the residual sodium ions in the samples and the EC and pH values were measured using the related devices (portable Jenway meters). The samples were weighed with a 3 decimal-accuracy digital scale and the DLS method (HORIBA model) was used to determine the particle size and gradation

of biochar particles.

Kinetics of sodium adsorption

Adsorption kinetics is an important factor in the design of adsorption tests and its models are either reaction-based (pseudo-first-order, pseudo-second-order and Elovich) or diffusion-based (intraparticle, internal-pore and external-film) (Sarici-Ozdemir, 2012). To study the biochar sodium adsorption kinetics, 0.75 gr of adsorbent was added to a 50 ml solution containing 10 g/l sodium in 10 separate containers and stirred with a 150 rpm-shaker at room temperature. Each container was then removed from the shaker in a 0-720 minute time-range and its sodium content was measured after passing the suspension through filter paper. The optimum contact time was measured by the adsorption kinetics test with MK_3N-BC-400-10 and the biochar-adsorbed sodium ions were found by Equation 1 from the difference between the initial and equilibrium ion concentrations in the remaining solution (Zhan et al., 2016):

$$q_e = \frac{(C_0 - C_e) \times V}{m} \quad (1)$$

Where C_0 and C_e are, respectively, the initial and equilibrium concentrations of the desired elements in the solution (mg/l), V is the suspension volume (l) and m is the adsorbent mass (g). The kinetics of the adsorption process have been studied using the pseudo-first-order, pseudo-second-order and diffusion kinetic models (Equations. 2, 3 and 4, respectively).

Pseudo-first-order kinetic model

The linear and non-linear pseudo-first-order kinetic equations are as follows:

$$\log(q_e - q_t) = log\ q_e - log\left(\frac{k_1 t}{2.303}\right) \quad (2)$$

$$q_t = q_e(1 - e^{-k_1 t}) \quad (3)$$

Where q_t is the ion adsorbed in time t (mg/g), q_e is the ion adsorbed in equilibrium time (mg/g), k_1 is the speed constant of the model (l/min) and t is time (min). Plotting log (q_e-q_t) versus t will yield a linear relation wherein k_1 and q_e are, respectively, the slope and y-intercept of the drawn line.

Pseudo-second-order kinetic model

The linear pseudo-second-order kinetic equation is as follows:

$$\frac{t}{q_t} = \frac{1}{k_2 q_e^2}\frac{t}{q_e} \quad (4)$$

$$q_t = \frac{k_2 q_e^2 t}{1 + k_2 q_e t} \quad (5)$$

Where q_e, q_t and t are those defined in Equation 1 and K_2 is the kinetic constant of the model (g/mg.min). Plotting t/q_t versus t will yield a linear relation wherein k_2 and q_e are, respectively, the slope and y-intercept of the drawn line (Deniz & Karaman, 2011).

Intraparticle diffusion kinetic model

The following equation, a diffusion-based model, describes competitive and multi-

stage adsorptions (first on the surface, then on the adsorbent):

$$q_t = k_p t^{0.5} + c \quad (6)$$

Where K_p is the model speed constant (mg/g.min$^{0.5}$) and C (mg/g) is the boundary layer thickness (the parameter that affects the increase or decrease of the diffusion rate). The slope of the q_t regression line versus $t^{0.5}$ will determine the K_{dif} parameter and its y-intercept will yield C (Ramachandran et al., 2011).

Isotherm adsorption models

Adsorption in a solid-liquid system involves extracting the solute from the solution and accumulating it on the adsorbent's surface, leading to a dynamic equilibrium between the solute concentration in the solution and on the adsorbent surface (Nikkhah et al., 2016). The adsorption isotherm is crucial for optimizing adsorbent usage as it illustrates how the pollutant interacts with the adsorbent (Crini et al., 2008). To investigate sodium adsorption, 0.75 g of adsorbent was added to containers with 50 ml of solutions at varying sodium concentrations (3, 5, 10, 15, 20, and 25 g/l). The mixture was stirred for 24 hours at 150 rpm, filtered, and the sodium concentration was measured; experiments were conducted on MK3N-BC-400-10. The Langmuir and Freundlich isotherm models were used to describe the biochar sodium-adsorption data.

Langmuir isotherm model

The Langmuir adsorption isotherm is found on several key assumptions: 1) Adsorption occurs at specific, homogeneous sites on the adsorbent, 2) each dye molecule occupies only one site at a time, 3) the adsorbent has a finite capacity, and 4) all sites are identical and possess similar energy. This isotherm serves as an experimental equation, indicating that as the adsorption sites on an adsorbent become occupied, the adsorption energy decreases exponentially (Khaled et al., 2009). The linear and nonlinear models of this isotherm are as follows:

$$\frac{c_e}{q_e} = \frac{1}{k_a Q_m} + \frac{1}{Q_m} \times c_e \quad (7)$$

$$q_e = \frac{Q_m K_a C_e}{1 + K_a C_e} \quad (8)$$

Where C_e is the equilibrium concentration of the liquid phase (mg/l), q_e is the adsorbent's absorption capacity (mg/g), Q_m is the maximum absorption capacity of the adsorbent (mg/g) and K_a is the absorption equilibrium constant (l/mg) which is related to the apparent energy of the absorption. Plotting C_e/q_e versus C_e should show a straight line with a slope of $1/Q_m$.

Freundlich isotherm model

Freundlich isotherm presents a relationship as follows for non-ideal and reversible adsorption. This experimental model can be used for multilayer adsorption with heterogeneous heat distribution and

adsorption on heterogeneous surfaces (Foo & Hameed., 2010). The linear and nonlinear models of this isotherm are as follows:

$$\ln q_e = \ln k_f + \frac{1}{n_f} \ln c_e \quad (9)$$

$$q_e = K_f C_e^{1/n_f} \quad (10)$$

where q_e is the adsorbent's absorption capacity at equilibrium time (mg/g), C_e is the adsorbent equilibrium concentration in solution (mg/l), K_f is the Friendlich constant (l/g) related to the bond energy and shows the amount of ions adsorbed on the adsorbent per unit equilibrium concentration, $1/n_f$ is the heterogeneity parameter and n_f is the deviation from the absorption line; adsorption is linear, chemical or physical if $n_f = 1$, $n_f < 1$ or $n_f > 1$, respectively.

To compare and evaluate the accuracy of the isothermal models and adsorption kinetics applied in this study, use was made of the correlation coefficient and standard estimation error (SSE) (Eq. 7, below):

$$SEE = \sqrt{\frac{\sum(Y_o - Y_p)^2}{N-1}} \quad (11)$$

Where Y_o and Y_p, are the observed and predicted values, respectively, and N is the number of samples.

Results and discussion

1.Activated nano biochar and Magnetic activated nano biochar

First, activated biochar (K-BC), activated nano biochar (KN-BC), and magnetic activated nano biochar (MKN) were used to remove sodium ions in different treatments. The percentage of sodium removal by these adsorbents is summarized in Table 1.

Table 1. The percentage of sodium removability by activated biochar, activated nano biochar & Magnetic activated nano biochar

		K-BC			KN-BC			MKN		
Initial concentration of sodium (g/l)		2	4	8	2	4	8	2	4	8
		Sodium removal (%)								
Microwave power	T(200W)	9.2	16.2	30.6	25.6	33.5	46.0	17.5	23.4	38.2
	T(400W)	13.3	22.8	39.1	26.9	40.6	53.3	21.5	34.8	47.5
	T(700W)	10.0	21.6	31.9	26.5	37.7	49.4	19.6	29.6	43.7

The study demonstrates that increasing the initial sodium concentration enhances sodium removability, with activated nano biochar being more effective than non-nano adsorbents. The largest effectiveness difference observed was 179.5% at 200 W microwave power and 2 g/l sodium concentration. As sodium concentration

increases, the difference in removability between nano and non-nano adsorbents decreases, with removability being 74.5% greater for nano adsorbents overall. Yang et al. (2018) tested the copper, lead, and zinc removability of corn stalk magnetic nano biochar and found it to be, respectively, 24.04, 54.04 and 16.74% with activated biochar and 80.96, 97.51 and 54.84% with activated nano biochar.. Nano biochar is more effective than non-nano biochar for removing contaminants because it has a much larger surface area and smaller, more numerous pores that improve adsorption. Its high reactivity enhances interactions with contaminants, and its nano-sized particles provide better access to solution. Furthermore, the surface charge of nano biochar strengthens electrostatic attraction with oppositely charged contaminants, thereby boosting its pollutant removal capabilities (Rajabi et al., 2023).

Magnetization reduces sodium removability by 18.8% compared to activated biochar, and the specific surface area of the adsorbent decreases from 745 to 459 m^2/g due to magnetization. In order to check the ability of the magnetic adsorbent, a strong magnet was used to separate the magnetized biochar particles from the solution (Xin et al., 2017). . When sodium concentrations increase, more sodium ions are available for biochar to interact with, making it easier to remove them. Higher sodium concentrations can help saturate the binding sites on biochar. This means that the biochar can effectively release other substances it might be holding onto, allowing for better removal of sodium (Medyńska-Juraszek et al., 2021).

An inverse relationship is noted between initial sodium concentration and removability reduction, with the highest removability reduction at 200 W and 2 g/l sodium concentration.

The optimal activator-to-adsorbent ratio for sodium removability is found to be 3 (K3) at 200 and 400 W. Increasing the ratio from 2 to 3 enhances removability, while further increases to 4 decrease it. Reducing the activator ratio from 3 to 2 decreases sodium removability by 4-8%, while increasing it to 4 reduces removability by 12-16% across different adsorbents.

2.Adsorption kinetics

To determine the sodium-adsorption kinetic model of the magnetic activated nano adsorbent, three kinetic models were used: 1) pseudo-first-order, 2) pseudo-second-order and 3) diffusion to study how sodium was adsorbed. The key differences between the pseudo-first-order and pseudo-second-order models in adsorption kinetics are mainly in how they describe the speed of adsorption. The pseudo-first-order model suggests that the rate of adsorption is proportional to the difference between the maximum adsorption capacity and the amount already adsorbed. In contrast, the

pseudo-second-order model indicates that the rate depends on the square of the amount adsorbed. The diffusion model focuses on how the movement of particles affects the adsorption process (Simonin, 2016). In model (1), the pollutant adsorption rate at any given time is directly proportional to the instantaneous pollutant concentration and the amount adsorbed to the adsorbent. Model (2) is based on the solid-phase adsorption capacity and assumes the adsorption rate is dependent on chemical adsorption. Model (3) examines the pollutant transfer into adsorbent based on the transfer rate of particles inside its pores (Li et al., 2022). Effects of contact-time on sodium removability were investigated for MK_3N-BC-200-10, MK_3N-BC-400-10 and MK_3N-BC-700-10.

Treatments at 200 and 700 W reached equilibrium after 480 minutes, while the 400 W treatment took 540 minutes. The adsorption rate decreases over time, approaching zero at equilibrium. The slope of the adsorption graph declines after 200 minutes for all adsorbents, indicating that sodium ions are initially adsorbed on the surface for up to 200 minutes. Once the surface is saturated, sodium ions penetrate the adsorbent cavities. As contact time increases, absorption improves due to more opportunities for interaction with functional groups. At equilibrium, sodium removal was 239 mg/g for 200 W, 260 mg/g for 400 W, and 201 mg/g for 700 W treatments.

Linear and nonlinear quasi-first-order kinetic models were drawn to the measured data for three absorbers; which Figure 2 presents the non-linear mode. The correlation coefficients for, respectively, MK_3N-BC-200-10, MK_3N-BC-400-10 and MK_3N-BC-700-10 are 0.97, 0.99 and 0.96, concluding that the pseudo-first-order kinetic model fits well with the real data, and the maximum and minimum constant adsorption rates relate to MK_3N-BC-700-10 and MK_3N-BC-400-10, respectively. The slope of the fitted line is negative in all three absorbers because, over time, more sodium is absorbed on the adsorbent surface. According to Figure 2, the nonlinear pseudo-first-order model has a satisfactory match with the real values.

Fitting the linear pseudo-second-order model to the measured data showed that the correlation coefficients were highly less than the pseudo-first-order model because during the first 60 min, the adsorption rate was high and more sodium was absorbed on the adsorbent surface, causing the t/q_t ratio to decrease, but after that, the t/q_t increased with a decrease in the adsorption rate.

As shown, for times less than 60 min, this kinetic model does not fit well to the measured data, but after 60 min, the correlation is better. Since adherence of the kinetic data to this model is an indication of chemical adsorption in the

adsorption process (Nikkhah et al., 2016), it can be concluded that, before 60 min, the dominant adsorption mechanism is not chemical.

In Figure 3, the non-linear second-order pseudo- model is presented. As shown in the Table 2, the non-linear pseudo-second-order model has provided far better results compared to the linear model.

The fitting of adsorption data using the intraparticle diffusion kinetic model reveals a strong correlation between the fitted line and measured values, indicating that sodium ion diffusion in the adsorbents occurs at a nearly uniform rate. This suggests that intraparticle diffusion is a significant factor in sodium adsorption from the start of the process. The MK3N-BC-400-10 treatment shows a longer time to reach equilibrium and a higher amount of adsorbed sodium (qt), indicating that its pore structure is more effective for sodium removal compared to the other two adsorbents (Fig. 4).

Table (2) lists the sodium-adsorption results of linear and non-linear kinetics models by magnetic activated nano biochar adsorbents. Comparing the sum of squared errors shows that, compared to the pseudo-second-order model, the pseudo-first-order model has estimated the maximum sodium adsorption closer to the real values. Considering the correlation coefficients and the sum of squared errors, the pseudo-first-order kinetic model and the intraparticle diffusion model conformed most to the measured data. According to Table 2, linear and nonlinear pseudo-first-order models have almost similar coloration values, although the linear model has a much lower SEE value and has more accurately estimated qe values. Compared to the linear model, the nonlinear pseudo-second-order model has a more accurate estimate of qe.

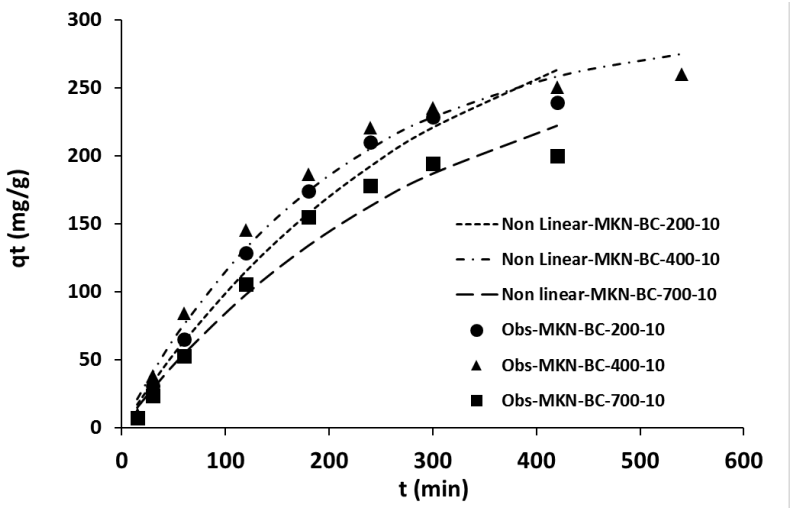

Fig 2. Fitting of the non-linear pseudo-first-order kinetic model to the measured values

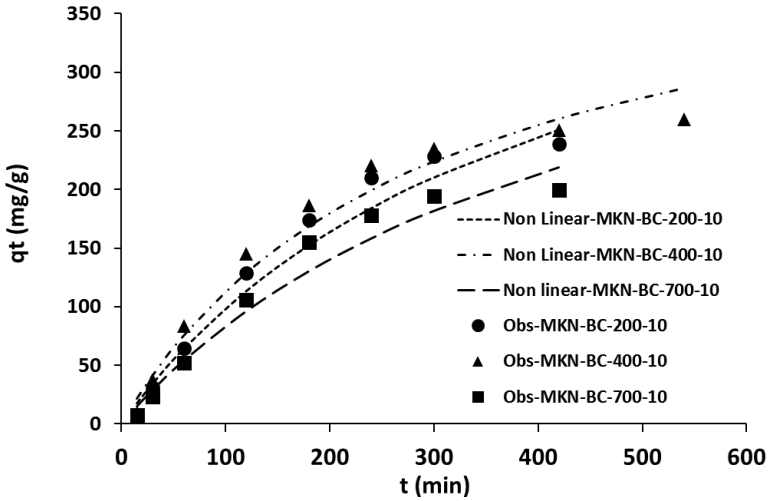

Fig 3. Fitting of the non-linear pseudo-second-order kinetic model to the measured values

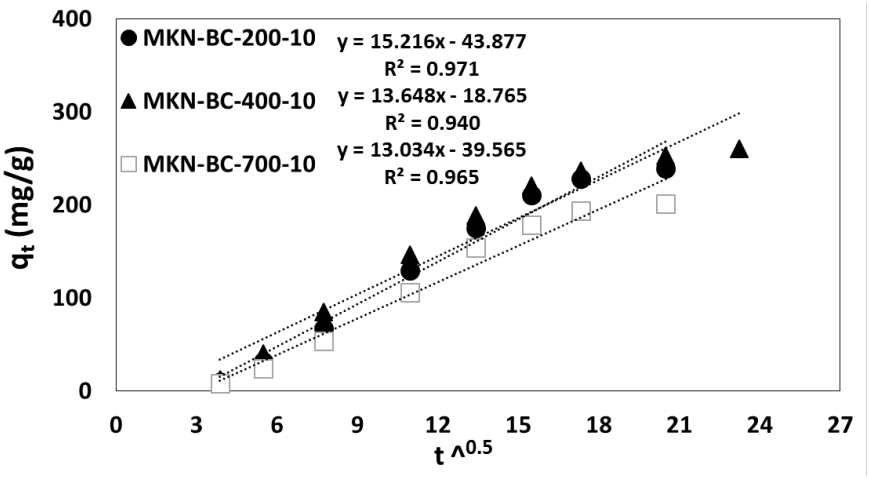

Fig 4. Fitting the intraparticle diffusion kinetic model to the measured values

3.Adsorption isotherm

According to isothermal curves that are used to describe the adsorption process at different concentrations, this process is strongly influenced by adsorption kinetics (Limousin et al., 2007). Although experimental isothermal models with 2, 3 or even 4 parameters can be used to understand the absorption mechanism, the 2-parameter ones are preferred due to their simplicity because if the data are well consistent with them, there is no need to use more complex models (Nadavala et al., 2009). Among isothermal models, since Langmuir and Friendlich are two common, widely used 2-parameter models (Mousavi et al., 2010), they have been used to study the adsorbents' behavior and capacity. The Langmuir and Freundlich isotherm models help explain how adsorbents like magnetically activated nano biochar behave and how much they can hold. The Langmuir model assumes that there's a maximum capacity for adsorption,

Table 2. Results of the fitting of kinetic linear and non-linear models to the measured values

	Linear				Non-linear			
pseudo-first-order	SSE	R2	K1	qe	SSE	R2	K1	qe
MK_3N-BC-200-10	0.091	0.9718	0.01036	313.1	14.665	0.975	0.003	349.408
MK_3N-BC-400-10	0.032	0.9969	0.00852	299.2	11.663	0.986	0.005	295.088
MK_3N-BC-700-10	0.111	0.9643	0.01105	278.6	13.997	0.969	0.003	291.948
pseudo-second-order	SSE	R2	k2	qe	SSE	R2	k2	qe
MK_3N-BC-200-10	0.289	0.3248	1.73E-06	769.2	16.72	0.96	5.1E-6	487.7
MK_3N-BC-400-10	0.292	0.7828	2.04E-06	833.3	16.56	0.97	7.8E-06	439.8
MK_3N-BC-700-10	0.319	0.2367	2.9E-07	1666.6	15.5	0.96	5.0E-06	448.8
pseudo-second-order (separated)	SSE	R2	k2	qe				
MK_3N-BC-200-10	0.038	0.9504	4.37E-06	555.5				
MK_3N-BC-400-10	0.041	0.9866	1.45E-05	370.3				
MK_3N-BC-700-10	0.070	0.8496	3.42E-06	555.5				
intraparticle diffusion	SSE	R2	Kp	c				
MK_3N-BC-200-10	0.011	0.9714	15.216	-43.877				
MK_3N-BC-400-10	0.019	0.9404	13.648	-18.765				
MK_3N-BC-700-10	0.011	0.9652	13.034	-39.565				

while the Freundlich model suggests that adsorption occurs on a heterogeneous surface with no limit. Key findings show that as sodium concentration increases, the adsorbent capacity and percentage sodium removal vary, providing insight into how effective the adsorbent is under different conditions and improving our understanding of the overall adsorption process (Khayyun, and Mseer, 2019).

Increasing the initial sodium concentration in the solution enhances sodium adsorption by the studied adsorbents. Specifically, raising the concentration from 3 to 25 g/l results in increased sodium absorption by 3, 3.5, and 2.6 times for the 200, 400, and 700 W treatments, respectively. The slope of the sodium removal curve shows a decreasing trend with higher initial concentrations. For the 400 W treatment, the slope remains unchanged below 10 g/l, while it decreases for the 200 and 700 W treatments, indicating that the 400 W treatment has a higher absorption capacity and is less affected by increased sodium concentration.

As sodium concentration rises, the slope reduces across all adsorbents, with the graphs becoming nearly horizontal for concentrations above 20 g/l. In terms of percent removal, increasing the initial concentration from 3 to 10 g/l shows little change, but raising it from 10 to 25 g/l leads to a reduction in percent removal by 52%, 46%, and 57% for the 200, 400, and 700 W treatments, respectively.

Among Langmuir model assumptions, one considers a monolayer adsorption process, another assumes a uniform adsorbent surface and a third omits interactions among adsorbed molecules (Senturk et al., 2009). The maximum sodium adsorption

capacities based on the Langmuir isothermal model are 344.8 mg/g for 200 W, 416.6 mg/g for 400 W, and 294.1 mg/g for 700 W.

Since the Langmuir isotherm model is highly consistent with the measured values and the correlation coefficient is above 99% for all three adsorbents, the sodium adsorption on their surfaces is done as a monolayer.

According to Figure 5, the nonlinear Langmuir model for the 400 W treatment did not have a good estimate of the real values. The Freundlich model assumes that particles are placed on the adsorbent surface in several layers. Figure (6) shows how the Freundlich model fits the data.

As shown in Figure 6, the correlation coefficients between the measured data and the Freundlich model are about 90%, which is lower than that of the Langmuir model. Table 3 presents the parameters of the Langmuir and Freundlich isothermal models. The nonlinear Freundlich model has a relatively accurate estimate of the real values for all treatments.

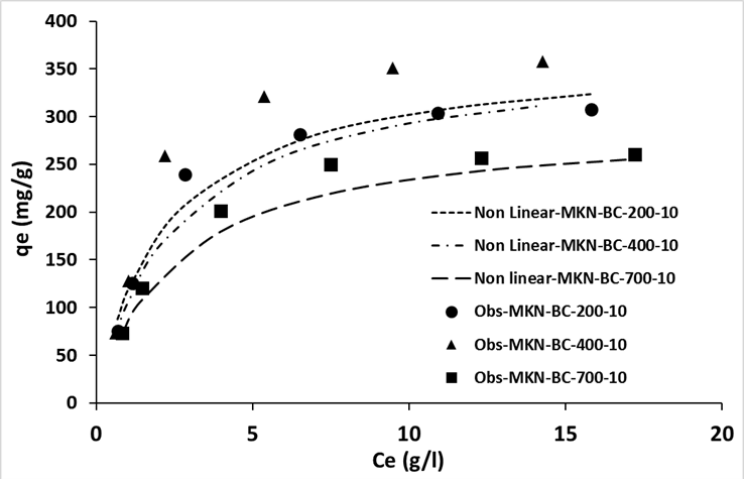

Fig 5. Fitting of the non-linear Langmuir isotherm model to the measured values

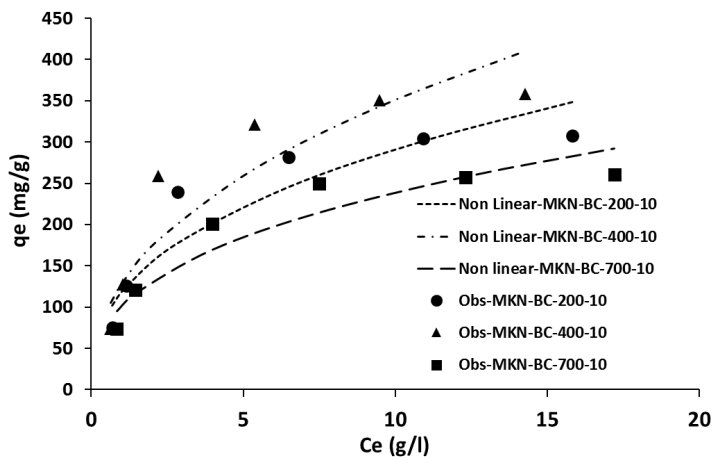

Fig 6. Fitting the non-linear Freundlich isotherm model to the measured values

Table 3. Fitting the adsorption isotherm models to the measured values

	Linear				Non-linear			
Langmuir	SSE	R^2	Ka	qe	SSE	R^2	Ka	qe
MK_3N-BC-200-10	1.28	0.9948	0.00055	344.82	17.42	0.96	0.00045	368.7
MK_3N-BC-400-10	1.23	0.9911	0.0005	416.66	61.88	0.81	0.00039	366.7
MK_3N-BC-700-10	1.55	0.9955	0.00047	294.11	18.77	0.94	0.00039	292.8
Freundlich	SSE	R^2	k_f	$1/n_f$	SSE	R^2	k_f	$1/n_f$
MK_3N-BC-200-10	0.2	0.8787	6.02	0.4258	38.86	0.86	7.74	0.39
MK_3N-BC-400-10	0.3	0.8698	5.06	0.4669	50.30	0.85	6.27	0.43
MK_3N-BC-700-10	0.16	0.9097	5.10	0.4206	27.33	0.89	7.76	0.37

As shown, since the average correlation coefficients are 0.9938 and 0.886 for the Langmuir and Freundlich models, respectively, the former is more consistent with the measured data. The n_f parameter is more than 1 for all three adsorbents; hence, the sodium adsorption process is mostly physical. According to table 3, Langmuir and Freundlich linear models have a better match with the real values. Also, the Langmuir model has estimated more accurate values than the Freundlich model.

The analysis of sugarcane bagasse biochar's efficiency in removing sodium ions from aqueous solutions highlights the importance of using nonlinear isotherm and kinetics models over linear ones for accurate representation. While linear models simplify the adsorption process and may lead to misinterpretations, nonlinear models better account for variations in adsorption capacity and dynamics, particularly at higher concentrations. Nonlinear modeling provides a superior fit to experimental data, enhances understanding of adsorption mechanisms, and is more adaptable to varying conditions. Overall, these models significantly improve insights into the effectiveness of biochar in environmental remediation, suggesting that future research should focus on nonlinear approaches for reliable data interpretation.

Conclusions

This study highlights the effectiveness of various biochar adsorbents, particularly activated nano biochar (KN-BC), in removing sodium ions from solutions. The results indicate that sodium removal efficiency increases with higher initial sodium concentrations, and nano biochar outperforms non-nano variants due to its larger surface area and enhanced adsorption properties. Although the magnetization of biochar slightly reduces sodium removability, the magnetically activated nano biochar (MKN) still demonstrates significant adsorption capabilities.

Kinetic studies reveal that the pseudo-first-order model best fits the adsorption data, suggesting that the initial adsorption mechanism is predominantly physical rather than chemical. The intraparticle diffusion model further supports the notion that sodium ion diffusion plays a critical role throughout the adsorption process.

Isothermal models, specifically Langmuir and Freundlich, were employed to analyze adsorption behavior. The Langmuir model showed a superior fit, indicating a monolayer adsorption process, while the Freundlich model suggested a heterogeneous surface with physical adsorption characteristics. The maximum sodium adsorption capacities were determined, with notable differences across treatments, emphasizing the influence of operational parameters such as microwave power.

Overall, the findings underscore the potential of using activated and nano biochar as effective adsorbents for sodium ion removal in wastewater treatment applications. Future research could explore optimizing conditions further and investigating the removal of other contaminants using similar methodologies. This work contributes valuable insights into the design and application of biochar-based materials for environmental remediation.

Abbreviation

BC: Biochar
N-BC: Nano biochar
Ka-BC: Activated non-nano biochar
KaN-BC: Activated nano biochar
MKaN-BC: Magnetic activated nano biochar
MKN-BC: Magnetic activated nano biochar
AN-BC: Activated nano biochar
KOH: Potassium hydroxide
W: Watts

Declarations

Ethical Approval

Not applicable.

Competing interests

On behalf of all authors, the corresponding author states that there is no conflict of interest.

Authors' contributions

Funding

Availability of data and materials

The datasets generated during and/or analyzed during the current study are available from the corresponding author on reasonable request.

Acknowledgments

This study was funded by the University of Lorestan, Lorestan, Iran. The support of this organization is appreciated. Also authors grateful of the Khuzestan Sugar Cane Research and Training Institute,

Khuzestan, Iran for its financial support.

References

Ayers, R. S., & Westcot, D. W. (1985). *Water quality for agriculture* (Vol. 29, p. 174). Rome: Food and agriculture organization of the United Nations. https://www.academia.edu/download/94774091/book_rs_ayers_and_wetscot.pdf

Bindhu, B. K., Shaji, H., Kuruvila, K. J., Nazerine, M., & Shaji, S. (2021, March). Removal of total hardness using low cost adsorbents. In *IOP Conference Series: Materials Science and Engineering* (Vol. 1114, No. 1, p. 012089). IOP Publishing. https://doi.org/10.1088/1757-899X/1114/1/012089

Cheng, S., Zhang, S., Zhang, L., Xia, H., Peng, J., & Wang, S. (2017). Microwave-Assisted Preparation of Activated Carbon from Eupatorium Adenophorum: Effects of Preparation Parameters. *High Temperature Materials and Processes*, *36*(8), 805-814. https://doi.org/ 10.1515/htmp-2015-0285

Chowdhury, T., Miah, J., & Banik, B. K. (2022). Low-Cost Salinity Treatment for Drinking Purpose Using Indigenous Materials. In *Advances in Civil Engineering: Select Proceedings of ICACE 2020* (pp. 37-44). Springer Singapore. https://doi.org/10.1007/978-981-16-5547-0_4

Crini, G., & Badot, P. M. (2008). Application of chitosan, a natural aminopolysaccharide, for dye removal from aqueous solutions by adsorption processes using batch studies: A review of recent literature. *Progress in polymer science*, *33*(4), 399-447. https://doi.org/10.1016/j.progpolymsci.2007.11.001

Crini, G., Lichtfouse, E., Wilson, L. D., & Morin-Crini, N. (2019). Conventional and non-conventional adsorbents for wastewater treatment. *Environmental Chemistry Letters*, *17*, 195-213. https://doi.org/10.1007/s10311-018-0786-8

Deniz, F., & Karaman, S. (2011). Removal of an azo-metal complex textile dye from colored aqueous solutions using an agro-residue. *Microchemical Journal*, *99*(2), 296-302. https://doi.org/10.1016/j.microc.2011.05.021

Dudley, L., Ben-Gal, A., & Shani, U. (2006, November). Influence of plant, soil and water properties on the leaching fraction. In *Agronomy Abstracts P* (Vol. 25711). https://scisoc.confex.com/crops/ 2006am/techprogram/P25711.HTM

Ehtaiwesh, A. F. (2022). The effect of salinity on nutrient availability and uptake in crop plants. *Scientific Journal of Applied Sciences of Sabratha University*, 55-73. https:// doi.org/10.47891/sabujas.v0i0.55-73.

Foo, K.Y., & Hameed, B.H. (2010). Insights into the modeling of adsorption isotherm systems. *Chemical Engineering Journal*, *156*(1), 2-10. DOI:10.1016/j.cej.2009.09.013

Hettiarachchi, E., Perera, R., Chandani Perera, A.D. L., & Kottegoda, N. (2016). Activated coconut coir for removal of sodium and magnesium ions from saline water. *Desalination and Water Treatment*, *57*(47), 22341-22352. DOI:10.1080/19443994.2015.1129649

Iwuozor, K. O., Emenike, E. C., Ighalo, J. O., Omoarukhe, F. O., Omuku, P. E., & Adeniyi, A. G. (2022). A review on the thermochemical conversion of sugarcane bagasse into biochar. *Cleaner Materials*, *6*, 100162. https://doi.org/10.1016/j.clema.2022.100162

Jamil, T.S., Ibrahim, H.S., Abd El-Maksoud,

I.H., & El-Wakeel, S.T. (2010). Application of zeolite prepared from Egyptian kaolin for removal of heavy metals: I. Optimum conditions. *Desalination*, *258*(1-3), 34-40. doi:10.1016/j.desal.2010.03.05

Kasraee, M., Dehghani, M. H., Mahvi, A. H., Nabizadeh, R., Arjmand, M. M., Salari, M., ... & Tyagi, I. (2022). Adsorptive removal of humic substances using cationic surfactant-modified nano pumice from water environment: Optimization, isotherm, kinetic and thermodynamic studies. *Chemosphere*, *307*, 135983. https://doi.org/10.1016/j.chemosphere.2022.135983

Kathiresan, M., & Sivaraj, P. (2016). Preparation and characterization of biodegradable sugarcane bagasse nano reinforcement for polymer composites using ball milling operation. *International Journal of Polymer Analysis and Characterization*, *21*(5), 428-435. doi:10.1080/1023666X.2016.1168061

Khaled, A., El Nemr, A., El-Sikaily, A., & Abdelwahab, O. (2009). Removal of Direct N Blue-106 from artificial textile dye effluent using activated carbon from orange peel: adsorption isotherm and kinetic studies. *Journal of hazardous materials*, *165*(1-3), 100-110. https://doi.org/10.1016/j.jhazmat.2008.09.122

Kharel, H. L., Sharma, R. K., & Kandel, T. P. (2016). Water hardness removal using wheat straw and rice husk ash properties. *Nepal Journal of Science and Technology*, *17*(1), 11-16. https://doi.org/10.3126/NJST.V17I1.25057

Khayyun, T. S., & Mseer, A. H. (2019). Comparison of the experimental results with the Langmuir and Freundlich models for copper removal on limestone adsorbent. *Applied Water Science*, *9*(8), 170. https://doi.org/10.1007/s13201-019-1061-2

Kietlińska, A., & Renman, G. (2005). An evaluation of reactive filter media for treating landfill leachate. *Chemosphere*, *61*(7), 933-940. https://doi.org/10.1016/j.chemosphere.2005.03.036

Li, D., Sun, L., Yang, L., Liu, J., Shi, L., Zhuo, L., Ye, T. and Wang, S., (2024). Adsorption behavior and mechanism of modified Pinus massoniana pollen microcarriers for extremely efficient and rapid adsorption of cationic methylene blue dye. *Journal of Hazardous Materials*, 465, p.133308. https://doi.org/10.1016/j.jhazmat.2023.133308

Li, Y., Gong, D., Zhou, Y., Zhang, C., Zhang, C., Sheng, Y., & Peng, S. (2022). Respiratory Adsorption of Organic Pollutants in Wastewater by Superhydrophobic Phenolic Xerogels. *Polymers*, *14*(8), 1596. https://doi.org/10.3390/polym14081596

Limousin, G., Gaudet, J. P., Charlet, L., Szenknect, S., Barthes, V., & Krimissa, M. (2007). Sorption isotherms: A review on physical bases, modeling and measurement. *Applied geochemistry*, *22*(2), 249-275. https://doi.org/10.1016/j.apgeochem.2006.09.010

López-Luna, J., Ramírez-Montes, L. E., Martinez-Vargas, S., Martínez, A. I., Mijangos-Ricardez, O. F., González-Chávez, M. D. C. A., ... & Vázquez-Hipólito, V. (2019). Linear and nonlinear kinetic and isotherm adsorption models for arsenic removal by manganese ferrite nanoparticles. *SN Applied Sciences*, *1*, 1-19. https://doi.org/10.1007/s42452-019-0977-3

Medyńska-Juraszek, A., Álvarez, M. L., Białowiec, A., & Jerzykiewicz, M. (2021). Characterization and sodium cations sorption capacity of chemically modified biochars produced from agricultural and forestry

wastes. *Materials*, *14*(16), 4714. https://doi.org/10.3390/ma14164714

Mehrabinia, P., & Ghanbari-Adivi, E. (2022). Examining nitrate surface absorption method from polluted water using activated carbon of agricultural wastes. *Modeling Earth Systems and Environment*, *8*(2), 1553-1561. DOI:10.1007/s40808-021-01221-5

Mehrabinia, P., Ghanbari-Adivi, E., Fattahi, R., Samimi, H. A., & Kermanezhad, J. (2021). Nitrate removal from agricultural effluent using sugarcane bagasse active nanosorbent. *Journal of Applied Water Engineering and Research*, *10*(3), 238-249. doi:10.1080/23249676.2021.1982030

Mehrabinia, P., Ghanbari-Adivi, E., Samimi, H. A., & Fattahi, R. (2022). Phosphate removal from agricultural drainage using biochar. *Water Conservation Science and Engineering*, *7*(4), 405-417. DOI: 10.1007/s41101-022-00150-3

Mousavi, A., Asadi, H., Esfandbod, M. (2010). Ion Exchange efficiency of nitrate removal from water 1- equilibrium sorption isotherms for nitrate on resin purolite a-400. *Water and Soil Science, 20*(4), 185. https://watersoil.tabrizu.ac.ir/article_1387.html. [In Persian]

Mubarak, A.A., Ilyas, R.A., Nordin, A.H., Ngadi, N. and Alkbir, M.F.M., (2024). Recent developments in sugarcane bagasse fibre-based adsorbent and their potential industrial applications: A review. International *Journal of Biological Macromolecules*, p.134165. https://doi.org/10.1016/j.ijbiomac.2024.134165

Musie, W., Gonfa, G., & Prabhu, S. V. (2023). Adsorption studies of sodium ions from aqueous solution with natural and sulfuric acid-treated bean seed husk. *Water, Air, & Soil Pollution*, *234*(3), 170. https://doi.org/10.1016/j.agwat.2008.04.010

Nadavala, S. K., Swayampakula, K., Boddu, V. M., & Abburi, K. (2009). Biosorption of phenol and o-chlorophenol from aqueous solutions on to chitosan–calcium alginate blended beads. *Journal of Hazardous Materials*, *162*(1), 482-489. https://doi.org/10.1016/j.jhazmat.2008.05.070

Naik, B. S., Panda, R. K., Nayak, S. C., & Sharma, S. D. (2008). Hydraulics and salinity profile of pitcher irrigation in saline water condition. *Agricultural water management*, *95*(10), 1129-1134. https://doi.org/10.1016/j.agwat.2008.04.010

Nasri, N.S., Zain, H.M., Sidik, H.U., Abdulrahman, A., & Rashid, N.M. (2017). Adsorption Isotherm breakthrough time of acidic and alkaline gases on treated porous synthesized KOH-FeCl 3. 6H 2 O sustainable agro-based material. *Chemical Engineering Transactions*, *61*, 1243-1248. Doi:10.3303/CET1761205

Nie, C., Yang, X., Niazi, N. K., Xu, X., Wen, Y., Rinklebe, J., ... & Wang, H. (2018). Impact of sugarcane bagasse-derived biochar on heavy metal availability and microbial activity: a field study. *Chemosphere*, *200*, 274-282. https://doi.org/10.1016/j.chemosphere.2018.02.134

Nikkhah, A. A., Zilouei, H., & Keshavarz, A. R. (2016). Effect of Structural Modification of Polyurethane Foam by Activated Carbon on the Adsorption of Oil Contaminants from Water. *Journal of Water and Wastewater; Ab va Fazilab (in persian)*, *27*(2), 84-93. [IN Persian]

Oliveira, E.A., Montanher, S.F., Andrade, A.D., Nobrega, J.A., & Rollemberg, M.C. (2005). Equilibrium studies for the sorption of chromium and nickel from aqueous solutions using raw rice bran. *Process Biochemistry*, *40*(11), 3485-3490. DOI:10.1016/j.

procbio.2005.02.026

Pearce, G. K. (2008). UF/MF pre-treatment to RO in seawater and wastewater reuse applications: a comparison of energy costs. *Desalination*, *222*(1-3), 66-73. https://doi.org/10.1016/j.desal.2007.05.029

Pourhakkak, P., Taghizadeh, A., Taghizadeh, M., Ghaedi, M., & Haghdoust, S. (2021). Fundamentals of adsorption technology. In *Interface science and technology* (Vol. 33, pp. 1-70). Elsevier. https://doi.org/10.1016/B978-0-12-818805-7.00001-1

Rahal, Z., Khechekhouche, A., Barkat, A., Sergeevna, S. A., & Hamza, C. (2023). Adsorption of Sodium in an Aqueous Solution in Activated Date Pits. Indonesian Journal of Science and Technology, 8(3), 387-412. DOI: 10.17509/ijost.v8i3.60066

Rajabi, M., Keihankhadiv, S., Suhas, Tyagi, I., Karri, R. R., Chaudhary, M., ... & Singh, P. (2023). Comparison and interpretation of isotherm models for the adsorption of dyes, proteins, antibiotics, pesticides and heavy metal ions on different nanomaterials and non-nano materials—a comprehensive review. Journal of Nanostructure in Chemistry, 13(1), 43-65. https://doi.org/10.1007/s40097-022-00509-x

Ramachandran, P., Vairamuthu, R., & Ponnusamy, S. (2011). Adsorption isotherms, kinetics, thermodynamics and desorption studies of reactive Orange 16 on activated carbon derived from Ananas comosus (L.) *carbon. Journal* of *Engineering and Applied Sciences*, *6*(11), 15-26.

Revellame, E.D., Fortela, D.L., Sharp, W., Hernandez, R. and Zappi, M.E.(2020). Adsorption kinetic modeling using pseudo-first order and pseudo-second order rate laws: A review. *Cleaner Engineering and Technology*, 1, p.100032. https://doi.org/10.1016/j.clet.2020.100032

Sarici-Ozdemir, C. (2012). Adsorption and desorption kinetics behaviour of methylene blue onto activated carbon. *Physicochemical problems of mineral processing*, *48*(2), 441-454.

Senturk, H. B., Ozdes, D., Gundogdu, A., Duran, C., & Soylak, M. (2009). Removal of phenol from aqueous solutions by adsorption onto organ modified Tirebolu bentonite: Equilibrium, kinetic and thermodynamic study. *Journal of hazardous materials*, *172*(1), 353-362. https://doi.org/10.1016/j.jhazmat.2009.07.019

Shang, H., Ouyang, T., Yang, F., & Kou, Y. (2003). A biomass-supported Na2CO3 sorbent for flue gas desulfurization. *Environmental Science &* Technology, *37*(11), 2596-2599. DOI: 10.1021/ es021026o

Simonin, J. P. (2016). On the comparison of pseudo-first order and pseudo-second order rate laws in the modeling of adsorption kinetics. *Chemical Engineering Journal*, *300*, 254-263. https://doi.org/10.1016/j.cej.2016.04.079

Singh, P., Garg, S., Satpute, S., & Singh, A. (2017). Use of rice husk ash to lower the sodium adsorption ratio of saline water. *International Journal of Current Microbiology and Applied Sciences*, *6*(6), 448-458. https://doi.org/10.20546/ijcmas.2017.606.052

Siyal, A. A., Siyal, A. G., & Abro, Z. A. (2002). Salt affected soils their identification and reclamation. https://www.cabidigitallibrary.org/doi/full/10.5555/20023095851

Wu, D., Sui, Y., He, S., Wang, X., Li, C., & Kong, H. (2008). Removal of trivalent chromium from aqueous solution by zeolite

synthesized from coal fly ash. *Journal of Hazardous Materials*, *155*(3), 415-423. https://doi.org/10.1016/j.jhazmat.2007.11.082

Wu, J., Huang, D., Liu, X., Meng, J., Tang, C., & Xu, J. (2018). Remediation of As (III) and Cd (II) co-contamination and its mechanism in aqueous systems by a novel calcium-based magnetic biochar. *Journal of hazardous materials*, *348*, 10-19. https://doi.org/10.1016/j.jhazmat.2018.01.011

Wu, J., Zhang, L., Xia, Y., Peng, J., Wang, S., Zheng, Z., & Zhang, S. (2015). Effect of microwave heating conditions on the preparation of high surface area activated carbon from waste bamboo. *High Temperature Materials and Processes*, *34*(7), 667-674. https://doi.org/10.1515/htmp-2014-0096

Xin, O., Yitong, H., Xi, C., & Jiawei, C. (2017). Magnetic biochar combining adsorption and separation recycle for removal of chromium in aqueous solution. *Water Science and Technology*, *75*(5), 1177-1184. https://doi.org/10.2166/wst.2016.610

Yang, F., Zhang, S., Sun, Y., Cheng, K., Li, J., & Tsang, D.C. (2018). Fabrication and characterization of hydropHilic corn stalk biochar-supported nanoscale zero-valent iron composites for efficient metal removal. *Bioresource Technology, 265*, 490-497. doi:10.1016/j.biortech.2018.06.029

Yılmazoğlu, M., 2021. Organic-Inorganic Ion Exchange Materials for Heavy Metal Removal from Water. Remediation of Heavy Metals, 179-198. https://doi.org/10.1007/978-3-030-80334-6_7

Zhan, T., Zhang, Y., Yang, Q., Deng, H., Xu, J., & Hou, W. (2016). Ultrathin layered double hydroxide nanosheets prepared from a waterin-ionic liquid surfactant-free microemulsion for pHospHate removal from aquatic systems. *Chemical Engineering Journal, 302*, 459-465. doi:10.1016/j.cej.2016.05.073